Noncollinear ferrimagnetism and anomalous Hall effects in Mn 4 N thin films

Yangkun He, Simon Lenne, Zsolt Gercsi, Gwenael Atcheson, Jack O'Brien, Daniel Fruchart, Karsten Rode, J. Coey

▶ **To cite this version:**

Yangkun He, Simon Lenne, Zsolt Gercsi, Gwenael Atcheson, Jack O'Brien, et al.. Noncollinear ferrimagnetism and anomalous Hall effects in Mn 4 N thin films. Physical Review B, 2022, 106 (6), pp.L060409. 10.1103/PhysRevB.106.L060409 . hal-04560516

HAL Id: hal-04560516
https://hal.science/hal-04560516v1

Submitted on 2 May 2024

HAL is a multi-disciplinary open access archive for the deposit and dissemination of scientific research documents, whether they are published or not. The documents may come from teaching and research institutions in France or abroad, or from public or private research centers.

L'archive ouverte pluridisciplinaire **HAL**, est destinée au dépôt et à la diffusion de documents scientifiques de niveau recherche, publiés ou non, émanant des établissements d'enseignement et de recherche français ou étrangers, des laboratoires publics ou privés.

Letter | Editors' Suggestion

Noncollinear ferrimagnetism and anomalous Hall effects in Mn_4N thin films

Yangkun He,[1,*] Simon Lenne,[1] Zsolt Gercsi,[1] Gwenael Atcheson,[1] Jack O'Brien,[1] Daniel Fruchart,[2] Karsten Rode,[1] and J. M. D. Coey[1]

[1]*School of Physics, CRANN, Trinity College, Dublin 2, Ireland*

[2]*Department of QUEST, Institut Néel, CNRS and UGA, 38042, Grenoble Cedex 9, France*

(Received 28 April 2022; revised 20 June 2022; accepted 4 August 2022; published 24 August 2022)

Thin films of Mn_4N and related ternary metallic perovskites with perpendicular anisotropy are interesting for spintronics, but their magnetic structures differ from the triangular ferrimagnetism of the bulk. A temperature-independent anomalous Hall conductivity of $-90\,\Omega^{-1}\,\mathrm{cm}^{-1}$ was found in Mn_4N films, in addition to the normal temperature-dependent contribution. Based on known spin structures of bulk Mn_3ZN compounds and the distance dependence of the Mn-Mn exchange for first- and second-neighbor Mn-Mn pairs, we propose a topological noncollinear spin structure for the Mn_4N films with perpendicular anisotropy. The Letter shows how a small change in symmetry of the spin structure can influence the magnetotransport properties of frustrated ferrimagnetic films.

DOI: 10.1103/PhysRevB.106.L060409

Frustrated magnets with a kagome lattice and the associated topology have attracted much attention for spintronics recently. Large anomalous Hall effects (AHEs) and anomalous Nernst effects were reported in Mn_3Sn [1] and Mn_3Ge [2] due to the Berry curvature induced by their triangular antiferromagnetism. Unlike ferromagnets, whose AHE depends on magnetization [Fig. 1(a)], these triangular antiferromagnets exhibit AHE derived from spin-orbit coupling (SOC) rather than their near-zero net moment [Fig. 1(b)] [3]. Collinear ferrimagnets with itinerant magnetic moments exhibit a magnetization-dependent AHE [Fig. 1(c)] [4], similar to ferromagnets which reverses sign at the compensation point where the net moment crosses zero. The above-mentioned cases have been well studied both experimentally and theoretically. However, we know little about the Hall conductivity of noncollinear ferrimagnets, although they are expected to combine features of both collinear ferrimagnets and noncollinear antiferromagnets as shown in Fig. 1(d) [3,5]. It is important to unravel the transport mechanism in order to design spintronic devices that make best use of these versatile noncollinear ferrimagnetic materials [6–9].

The noncollinear manganese nitride Mn_4N and related ternary alloys $Mn_{4-x}Z_xN$ (Z is a nonmagnetic dopant) with the perovskite structure are attractive because of the opportunities they offer [6] for combining compensated ferrimagnetism [10,11] with good electrical and thermal transport properties [12], strain sensitivity [13], first-order phase transitions [14], magnetic skyrmions [15], and magneto-optic spintronics [16]. Bulk Mn_4N crystallizes in space-group $Pm\bar{3}m$ where N is in octahedral coordination at the body-centered interstitial site of a Mn face-centered-cubic lattice. The metallic compound was originally thought to be a collinear ferrimagnet with a small net moment of $1.1\mu_B$ per formula unit [17] ($3.8\mu_B$ for Mn in the $1a$-corner site and $-0.9\mu_B$ for each Mn in the $3c$-face-centered sites). The unusual thermomagnetic magnetization curve of the end member and the absence of compensation that would have been expected for collinear ferrimagnetism based on the mean-field model [18] raised questions about the true magnetic structure. A later neutron study with polarization analysis revealed frustrated noncollinear ferrimagnetism that combines a 120° triangular antiferromagnetism of the projection of Mn $3c$-site moments onto the (111) plane and a ferrimagnetic ordering of the collinear $1a$ sublattice and the ferromagnetic component of the $3c$ moments along the [111]-easy direction [19]. The triangular in-plane antiferromagnetism, confirmed by subsequent density functional theory (DFT) calculations [11,20] is a result of the frustration of the antiferromagnetic coupling arising from the short distance (∼0.270 nm) between the nearest-neighbor Mn^{3c} atoms in the (111)-kagome planes [11].

The easy axis in high-quality thin films grown on MgO switches to [001] with perpendicular anisotropy due to tensile strain at the interface between substrate and film [21–23]. A slight tetragonal distortion breaks the cubic symmetry of the bulk, splitting the $3c$ sites into inequivalent $2e$ and $1c$ sites in space-group $P4/mmm$. Up to now, most studies of Mn_4N thin films have ignored the frustration of the antiferromagnetic interactions [11,24] and treated them as simple collinear ferrimagnets as shown in Fig. 2(a). Since misleading inferences of compensation are likely to be drawn from false assumptions (Mn_4N does *not* exhibit compensation), it is important to build a reasonable noncollinear model for the magnetic structure of the thin films. Here, the collinear and possible frustrated noncollinear spin structures are discussed in terms of the known noncollinear structures of related bulk compounds and the sign of the Mn-Mn exchange interactions. A temperature-independent anomalous Hall effect reveals the presence of a topological noncollinear spin structure.

*heya@tcd.ie

 ©2022 American Physical Society

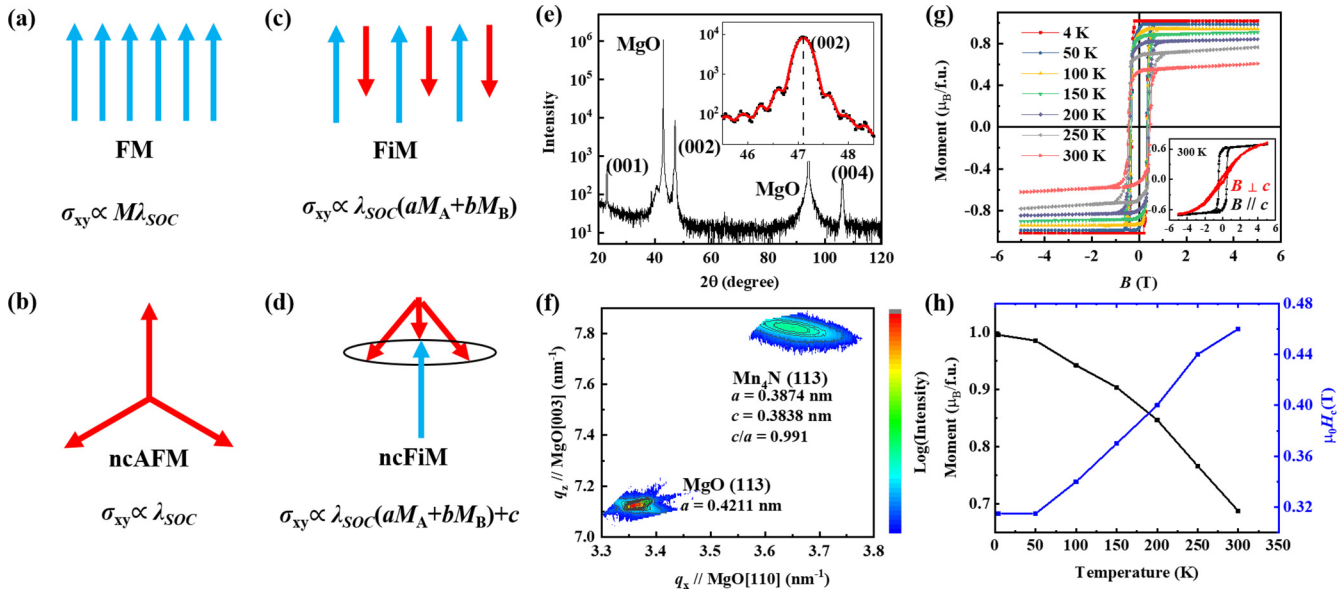

FIG. 1. (a)–(d) Anomalous Hall effect on different magnetic structures: (a) Ferromagnet (FM); (b) Noncollinear triangular antiferromagnet (ncAFM); (c) Collinear ferrimagnet (FiM); (d) Noncollinear, triangular ferrimagnet (ncFiM). M, M_A, and M_B refer to the ferromagnetic magnetization and ferrimagnetic sublattice magnetizations; $a\lambda_{SOC}$ and $b\lambda_{SOC}$ refer to spin-orbital coupling strengths on the two sublattices; c is the anomalous Hall effect arising from a topological noncollinear structure. (e) XRD pattern of Mn_4N films grown on a MgO substrate. The inset shows the enlarged (002) peak. (f) Reciprocal space mapping of the (113) peak. (g) Magnetization curves at different temperatures. (h) Temperature-dependent saturation moment and coercivity.

Thin films of Mn_4N were deposited by reactive sputtering of Mn with N_2 on MgO (001) substrates heated to ~710 K at a deposition rate of 2 nm/min. The ratio of Ar to N_2 was 20:1. Films were cooled in the Ar/N_2 gas environment before depositing a 4-nm-thick capping layer of SiO_2 at room temperature. The crystal structure was characterized by x-ray diffraction (XRD). The film thickness was determined by x-ray reflectivity (XRR) and from Laue fringes around the (002) peak. Hall bars (50-μm long and 10-μm wide) were patterned by ultraviolet lithography and Ar-ion milling. Transport measurements were conducted in a Multimag variable-field permanent magnet system [25] on Hall bars with a DC current of 1 mA. Magnetization measurements were made using a superconducting quantum interference device magnetometer (Quantum Design). The substrate background was removed by subtraction.

The Laue fringes in the XRD pattern of the highly orientated (001) film in Fig. 1(e) indicate the high film quality, despite the lattice mismatch with the MgO. The film thickness was 27.8 nm. Reciprocal space mapping in Fig. 1(f) shows the crystallographic relationship between the substrate and the film, (113) Mn_4N ∥ (113) MgO. The lattice constants are

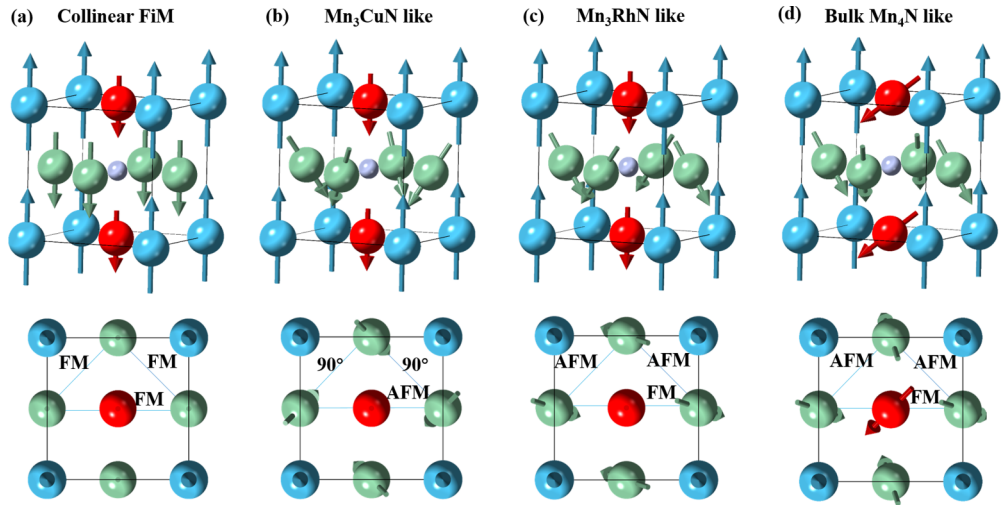

FIG. 2. Possible magnetic structures of Mn_4N films with a side view (top row) and a top view (bottom row). Blue, red, green, and small gray atoms refer to Mn^{1a}, Mn^{1c}, Mn^{2e}, and N, respectively. The exchange interactions for nearest-neighbor (NN) and next-nearest-neighbor (NNN) Mn^{2e} atoms are marked. AFM and FM for antiferromagnetic and ferromagnetic, respectively. Only the bulk Mn_4N-like model has exchange interactions that are consistent with the Mn-Mn distances; it is the most likely structure.

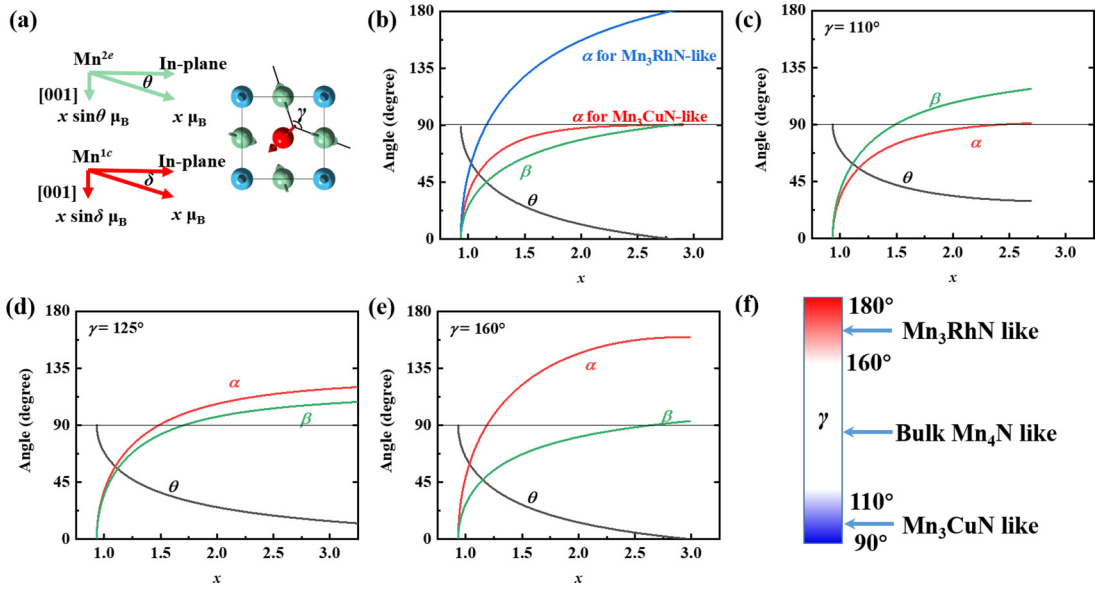

FIG. 3. (a) Schematic of the angles θ, δ, and γ. (b) Relationships among α, β, θ, and the moment x for Mn_3CuN-like and Mn_3RhN-like models. (c)–(e) Relationships between α, β, and θ and the moment x for the bulk Mn_4N-like model with $\gamma = 110°$, 125°, and 160°, respectively. Antiferromagnetic exchange between the nearest Mn^{2e}-Mn^{2e} and Mn^{2e}-Mn^{1c} requires $\alpha > 90°$ and $\beta > 90°$, respectively. (f) The magnetic model changes from Mn_3CuN-like to Mn_3RhN-like with increasing γ.

$a = 0.387(4)$ and $c = 0.383(8)$ nm with $c/a = 0.99(1)$. A 2.6-nm-thick layer of Mn oxide was identified at the interface between the substrate and the film from fitting XRR data. Details are shown in Supplemental Material Fig. S1 [26].

Figure 1(g) shows the *M*-*H* curves of a Mn_4N film at temperatures between 300 and 4 K. Hysteresis loops are square, indicating perpendicular magnetic anisotropy with a coercivity of about 0.4 T. The magnetization increases from $0.69\mu_B$/f.u. at 300 K to $1.0\mu_B$/f.u. at 4 K without any compensation. The magnetization is a little lower in the film than in the bulk ($1.1\mu_B$/f.u.). The anisotropy field $\mu_0 H_a$ at room temperature is 4 T, giving a magnetocrystalline anisotropy of 170 kJ m^{-3}. Figure 1(h) shows the opposite variation of magnetization and coercivity with temperature. The unusually rapid decline of the magnetization from 4 to 100 K without compensation at higher temperature is a sign of a noncollinear structure [11,18]. T_C is estimated to be 750 ± 20 K by comparison with the temperature dependence of the magnetization of bulk material [11].

Given the slightly tetragonal crystal structure associated with [001]-perpendicular anisotropy, we consider possible noncollinear magnetic structures of Mn_4N films based on the distance dependence of Mn-Mn exchange interactions. Numerous reports of magnetic structures for Mn_3ZN metallic perovskites can help [27] to build a model of quadratic antiferromagnetism with four noncollinear Mn^{2e} sublattices. The simplest noncollinear model in Fig. 2(b) is based on Mn_3CuN, a rare noncollinear ferromagnet in the Mn_3ZN family where Cu on 1*a* sites has no moment. The compound is tetragonal with $c/a = 0.99$, similar to the Mn_4N films. The magnetic ordering temperature ($T_C = 140$ K) is low compared to its antiferromagnetic ($T_N = 200$–300 K) or ferrimagnetic ($T_C > 500$ K) counterparts. The net moment of $1.3\mu_B$ per formula unit along [001] originates mainly from Mn on 1*c* sites ($0.65 \pm 0.15\mu_B$). The moment of the 2*e* site Mn ($2.85\mu_B$) is aligned at nearly 90° to [001] with only a small component of $0.2 \pm 0.1\mu_B$/Mn parallel to the 1*c*-site Mn moment [27]. The 2*e*-2*e* and 2*e*-1*c* exchange is weak because of the 90° coupling, which explains the low T_C. By replacing Cu on 1*a* sites by Mn, which couples antiferromagnetically with 1*c* and 2*e* site Mn atoms along [001], a first Mn_3CuN-like model of the magnetic structure for the (001) Mn_4N film is established. The tilt angle of Mn^{2e} moments out of the (001) plane is larger than in Mn_3CuN.

To account for the ferrimagnetic moment of $1.0\mu_B$/f.u. in the [001] direction in this model, the magnetic moment for Mn^{2e} and Mn^{1c} (supposing both are $x\mu_B$) satisfies

$$3.8 - x(2\sin\theta + 1) = 1.0, \tag{1}$$

where $3.8\mu_B$ is the moment of Mn^{1a} [19] and θ is the tilt angle of the 2*e* site moments [see Fig. 3(a)]. The angle α between moments of two nearest-neighbor Mn^{2e} atoms is $\arccos(\sin^2\theta)$, and the angle β between the moments of Mn^{2e} and Mn^{1c} is (90°–θ). The relationship among θ, α, and β for a given moment x is plotted in Fig. 3(b). There are two problems with this model: (1) angle α is close to 90°, giving an unreasonably small exchange energy between two nearest-neighbor Mn^{2e} atoms, and it is not a favored arrangement of spins. (2) The angle β is smaller than 90°, indicating a ferromagnetic interaction between Mn^{2e} and Mn^{1c}. Since an antiferromagnetic interaction is expected for this short Mn-Mn distance, the model needs to be refined.

The first problem is solved by rearranging the in-plane component of Mn^{2e}. In the revised model, the in-plane component is antiparallel for nearest-neighbor Mn^{2e} atoms [Fig. 2(c)] as in the Mn_3RhN structure [27]. Equation (1) is still valid in this Mn_3RhN-like model, whereas $\beta = 90°$–θ and $\alpha = 180°$–2θ as shown in Fig. 3(b). Since α is larger than 90°, the exchange between two nearest-neighbor Mn^{2e} atoms is antiferromagnetic. In addition, the moment for next-nearest

TABLE I. Exchange interaction between different Mn sites.

Model	1*a*-1*a*	1*a*-1*c*	1*a*-2*e*	1*c*-1*c*	1*c*-2*e*	2*e*-2*e* NN	2*e*-2*e* NNN
Distance (nm)	0.3838	0.2739	0.2727	0.3838	0.2727	0.2739	0.3874
Collinear FiM	FM	AFM	AFM	FM	FM	FM	FM
Mn_3CuN-like	FM	AFM	AFM	FM	90°	90°	AFM
Mn_3RhN-like	FM	AFM	AFM	FM	FM	AFM	FM
Bulk Mn_4N-like	FM	AFM	AFM	FM	AFM	AFM	FM

neighbor (NNN) Mn^{2e} is parallel, indicating ferromagnetic exchange for the large Mn-Mn NNN distance of ∼0.38 nm. Although the interaction for Mn^{2e} is more reasonable, angle β between Mn^{2e} and Mn^{1c} is still less than 90°. Further improvement is needed.

In both of these models, the moment of Mn^{1c} is along [001], and the net in-plane component of Mn^{2e} is zero. By tilting the moment of Mn^{1c}, a new bulk Mn_4N-like model is established as shown in Fig. 2(d). The tilt angle δ away from (001) for the Mn^{1c} moments satisfies the relationship for a ferrimagnetic structure,

$$3.8 - x(2\sin\theta + \sin\delta) = 1.0. \tag{2}$$

If γ is the angle between the in-plane components of moments of two nearest-neighbor Mn^{2e} atoms shown in Fig. 3(a), then the in-plane antiferromagnetism is described by $\delta = \arccos[2\cos\theta\cos(\gamma/2)]$. Angles α and β are $\arccos[\sin^2\theta + \cos^2\theta\cos\gamma]$ and $\arccos[\sin\theta\sin\delta - \cos\theta\cos(\gamma/2)\cos\delta]$, respectively. From these equations, we can plot the relationship between x and the angles for a given value of γ. Figures 3(c)–3(e) show the relationship for $\gamma = 110°$, 125°, and 160°. When $\gamma < 110°$, α is smaller than 90°, giving a structure similar to the Mn_3CuN-like model. When $\gamma > 160°$, β is smaller than 90°, giving a structure similar to the Mn_3RhN-like model. The Mn_3CuN-like and Mn_3RhN-like models are the two extreme cases with $\delta = 90°$ and $\gamma = 90°$ or 180° respectively.

Table I summarizes the interactions in the four different magnetic models we have considered for Mn_4N films. The sign of exchange in the first four columns is identical, and the main difference is related to the exchange between Mn^{2e} and Mn^{1c}. The bulk Mn_4N-like model with $110° < \gamma < 160°$ has exchange interactions that respect the Mn-Mn distances; the coupling of the nearest-neighbor (∼0.27-nm) and the next-nearest-neighbor (∼0.38-nm) Mn atoms are antiferromagnetic and ferromagnetic, respectively. We also include a recent DFT result that the lattice parameter for the noncollinear model yields values closer to the experimental value [11].

We now turn to the anomalous Hall effect to highlight the role of noncollinearity. Theoretical studies of Hall effects due to noncollinear antiferromagnetism have been reported for Mn_3ZN with several nonmagnetic elements Z [5,28]. For a triangular ferrimagnet, reversal of the applied magnetic field simultaneously flips the out-of-plane net magnetization and the in-plane spin structure. The tilted noncollinear spin structures with reversed tilt angle exhibit anomalous Hall effects of opposite sign [5]. Therefore, an anomalous Hall effect in Mn_4N arises from both ferrimagnetism $\sigma_{xy}^{\mathrm{FiM}}$ and triangular antiferromagnetism $\sigma_{xy}^{\mathrm{AFM}}$ [29]. Note that in the bulk Mn_4N-like model, the in-plane directions for Mn^{1c} and Mn^{2e} are not fixed by exchange. They can rotate coherently whereas retaining the same exchange forming a Γ^{5g}-like or Γ^{4g}-like structure, in Bertaut's notation [30]. The Γ^{4g}-like structure with a radial spin structure in the triangles is topological [5] and exhibits a temperature-independent topological contribution to the anomalous Hall effect, whereas Γ^{5g}-like with a toroidal spin structure (see $Co_3Sn_2S_2$ [31]) exhibits no additional anomalous Hall effect. A more detailed discussion about the spin structure, topology, and their relation to the anomalous Hall effect is given in Supplemental Material Fig. S2 [26]. The symmetry is analyzed in Ref. [28].

For itinerant ferrimagnets, the intrinsic anomalous Hall conductivity is proportional to the net magnetization [4]. The contribution of the Hall conductivity can be expressed as

$$\sigma_{xy} = \sigma_{xy}^{\mathrm{FiM}}(M) + \sigma_{xy}^{\mathrm{AFM}} + \sigma_{xy}^{\mathrm{NHE}}(B). \tag{3}$$

The last term is the normal Hall conductivity (a function of applied magnetic-field B, which is negligibly small in metallic films.

The transverse resistivity ρ_{xy} is plotted as a function of magnetic field in Fig. 4(b). At room temperature, ρ_{xy} is $-3.25\,\mu\Omega\,\mathrm{cm}$, whereas at 27 K it decreases to $-0.39\,\mu\Omega\,\mathrm{cm}$. Considering the longitudinal resistivity ρ_{xx} that decreases from 89 to 25 $\mu\Omega$ cm in the same temperature range shown in Fig. 4(a), the Hall conductivity calculated by $\sigma_{xy} = -\rho_{xy}/\rho_{xx}^2$ at different temperatures is plotted in Fig. 4(c). It remains constant at about $620\,\Omega^{-1}\,\mathrm{cm}^{-1}$ below 50 K and decreases linearly during heating to $410\,\Omega^{-1}\,\mathrm{cm}^{-1}$ at 300 K, following the trend of the magnetization. A maximum Hall angle (σ_{xy}/σ_{xx}) of 3.6% was found at room temperature, larger than that of the common 3*d* ferromagnets Fe, Co, and Ni with similar spin-orbit coupling [32].

σ_{xy} as a function of the magnetization is plotted in Fig. 4(d). A linear trend is clearly shown, accompanied with a negative intercept of $-90\,\Omega^{-1}\,\mathrm{cm}^{-1}$ which is the Hall contribution from noncollinear spin structure $\sigma_{xy}^{\mathrm{AFM}}$. As a result, the $\sigma_{xy}^{\mathrm{FiM}}$ is found to be $710\,\Omega^{-1}\,\mathrm{cm}^{-1}$ at low temperature and $500\,\Omega^{-1}\,\mathrm{cm}^{-1}$ at 300 K. Experiments on two different samples gave identical results. The intercept is not a result of experimental error because errors in the transport measurements due to dimensions of the Hall bar or in the magnetization due to the thickness/area of the film will only change the slope of the curve. Nor can the intercept be attributed to an error in the temperature reading because for the line to pass through the origin, a temperature deviation of 100 K would be required, far exceeding our estimated error of ±5 K. An anomalous Nernst effect is also excluded as shown in Supplemental Material

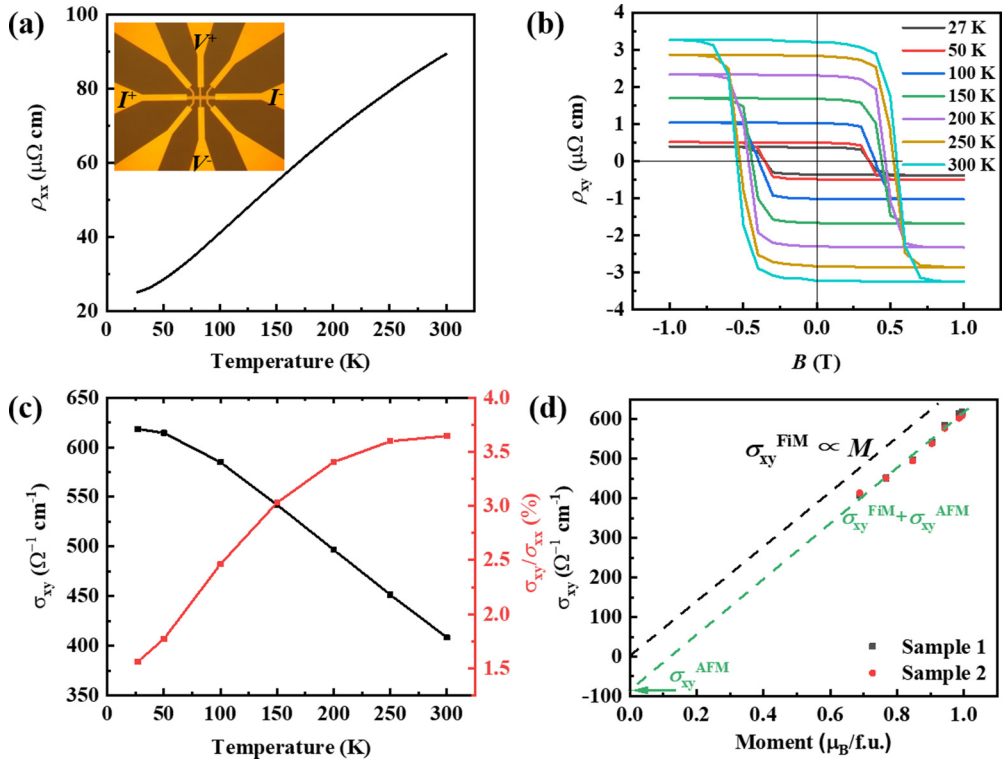

FIG. 4. Transport properties of Mn_4N film. (a) Longitudinal resistivity as a function of temperature. The inset shows the image of the 10-μm-wide Hall bar. (b) ρ_{xy} at different temperatures. (c) Hall conductivity and Hall angle as a function of temperature. (d) Hall conductivity as a function of the magnetization (obtained at 1 T). The linear fit (green line) gives a negative intercept of $\sigma_{xy}^{AFM} = -90\,\Omega^{-1}\,cm^{-1}$, which is the temperature-independent topological contribution.

Fig. S3 [26]. σ_{xy}^{AFM} is, therefore, a sign of a topological noncollinear spin structure. Larger anomalous Hall effects have been reported in the hexagonal noncollinear antiferromagnets Mn_3Ge ($450\,\Omega^{-1}\,cm^{-1}$) [2] and Mn_3Sn ($100\,\Omega^{-1}\,cm^{-1}$) [1], but the σ_{xy}^{AFM} of $-90\,\Omega^{-1}\,cm^{-1}$ in our Mn_4N film is similar to other cubic noncollinear antiferromagnets Mn_3Pt ($98\,\Omega^{-1}\,cm^{-1}$) [33] and Mn_3Ir ($-40\,\Omega^{-1}\,cm^{-1}$) [34].

In conclusion, it is a challenge to determine complex magnetic spin structures in thin films. Neutron diffraction is at the limit of its sensitivity due to the small sample size. Density functional theory calculations may be unable to distinguish topological and nontopological spin structures that differ by spin-orbit coupling/anisotropy energies of several μeV/atom. X-ray magnetic circular dichroism struggles to distinguish Mn atoms in inequivalent sites. Our methodology makes use of what is already known about magnetic structures in various bulk Mn_3ZN metallic perovskites and the systematic distance dependence of the sign of direct Mn-Mn exchange in metals to infer a tetragonal magnetic structure with topological and nontopological variants for Mn_4N thin films grown on MgO. The tetragonal distortion of the film breaks the cubic symmetry, leading to perpendicular anisotropy which is important for magnetotransport and magneto-optic measurements. We propose a noncollinear frustrated ferrimagnetic structure based on exchange interactions that are antiferromagnetic and ferromagnetic for nearest and next-nearest neighbors, respectively. The difference is that the in-plane antiferromagnetism is triangular in the bulk where [111] is the easy direction but quadratic in thin films with a [001] easy direction. The topological variant of the noncollinear spin structure (Γ^{4g}-like structure) was favored by separating a temperature-independent contribution to the anomalous Hall effect $\sigma_{xy}^{AFM} = -90\,\Omega^{-1}\,cm^{-1}$ from the temperature-dependent contribution, $\sigma_{xy}^{FiM} = 710\,\Omega^{-1}\,cm^{-1}$ at low temperature. Our Letter provides both evidence for a quadratic spin structure with topological character in Mn_4N and insight into the behavior of thin films of triangular ferrimagnets.

This work was supported by the Science Foundation Ireland under the MANIAC, SFI-NSF China Project (Grant No. 17/NSFC/5294) and ZEMS Project Grant No. 16/IA/4534.

[1] S. Nakatsuji, N. Kiyohara, and T. Higo, Large anomalous Hall effect in a non-collinear antiferromagnet at room temperature, Nature (London) **527**, 212 (2015).

[2] A. K. Nayak, J. E. Fischer, Y. Sun, B. Yan, J. Karel, A. C. Komarek, C. Shekhar, N. Kumar, W. Schnelle, J. Kübler, C. Felser, and S. S. P. Parkin, Large anomalous Hall effect driven by a nonvanishing berry curvature in the noncolinear antiferromagnet Mn_3Ge, Sci. Adv. **2** e1501870 (2016).

[3] Y. Zhang, Y. Sun, H. Yang, J. Železný, S. P. P. Parkin, C. Felser, and B. Yan, Strong anisotropic anomalous Hall effect and spin

Hall effect in the chiral antiferromagnetic compounds Mn_3X (X = Ge, Sn, Ga, Ir, Rh, and Pt), Phys. Rev. B **95**, 075128 (2017).

[4] A. Husmann and L. J. Singh, Temperature dependence of the anomalous Hall conductivity in the heusler alloy Co_2CrAl, Phys. Rev. B **73**, 172417 (2006).

[5] O. Busch, B. Göbel, and I. Mertig, Microscopic origin of the anomalous Hall effect in noncollinear kagome magnets, Phys. Rev. Research **2**, 033112 (2020).

[6] J. M. D. Coey, D. Givord, and D. Fruchart, Metallic nitride and carbide perovskites: History and prospects, ECS J. Solid State Sci. Technol. **11**, 055002 (2022).

[7] T. Suemasu, L. Vila, and J-P Attané, Present status of rare-earth free ferrimagnet Mn_4N and future prospects of Mn_4N-based compensated ferrimagnets, J. Phys. Soc. Jpn. **90**, 081010 (2021).

[8] Z. Zhang and W. Mi, Progress in ferrimagnetic Mn_4N films and its heterostructures for spintronics applications, J. Phys. D: Appl. Phys **55**, 013001 (2022).

[9] H. K. Singh, I. Samathrakis, N. M. Fortunato, J. Zemen, C. Shen, O. Gutfleisch, and H. Zhang, Multifunctional antiperovskites driven by strong magnetostructural coupling, NPJ Comp. Mater. **7**, 98 (2021).

[10] S. Ghosh, T. Komori, A. Hallal, J. P. Garcia, T. Gushi, T. Hirose, H. Mitarai, H. Okuno, J. Vogel, M. Chshiev, J. Attané, L. Vila, T. Suemasu, and S. Pizzini, Current-Driven domain wall dynamics in ferrimagnetic nickel-doped Mn_4N films: Very large domain wall velocities and reversal of motion direction across the magnetic compensation point, Nano Lett. **21**, 2580 (2021).

[11] R. Zhang, Y. He, D. Fruchart, J. M. D. Coey, and Z. Gercsi, Rare-earth-free noncollinear metallic ferrimagnets $Mn_{4-x}Z_xN$ with compensation at room temperature, Acta Mater. **234**, 118021 (2022).

[12] S. Isogami, K. Masuda, Y. Miura, N. Rajamanickam, and Y. Sakuraba, Anomalous Hall and Nernst effects in ferrimagnetic Mn_4N films: Possible interpretations and prospects for enhancement, Appl. Phys. Lett. **118**, 092407 (2021).

[13] D. Matsunami, A. Fujita, K. Takenaka, and M. Kano, Giant barocaloric effect enhanced by the frustration of the antiferromagnetic phase in Mn_3GaN, Nature Mater. **14**, 73 (2015).

[14] D. Boldrin, E. Mendive-Tapia, J. Zemen, J. B. Staunton, T. Hansen, A. Aznar, J. Tamarit, M. Barrio, P. Lloveras, J. Kim, X. Moya, and L. F. Cohen, Multisite Exchange-Enhanced Barocaloric Response in Mn_3NiN, Phys. Rev. X **8**, 041035 (2018).

[15] C. T. Ma, T. Q. Hartnett, W. Zhou, P. V. Balachandran, and S. J. Poon, Tunable magnetic skyrmions in ferrimagnetic Mn_4N, Appl. Phys. Lett. **119**, 192406 (2021).

[16] T. Gushi, M. J. Klug, J. P. Garcia, S. Ghosh, J. Attané, H. Okuno, O. Fruchart, J. Vogel, T. Suemasu, S. Pizzini, and L. Vila, Large current driven domain wall mobility and gate tuning of coercivity in ferrimagnetic Mn_4N thin films, Nano Lett. **19**, 8716 (2019).

[17] W. J. Takei, R. R. Heikes, and G. Shirane, Magnetic structure of Mn_4N-type compounds, Phys. Rev. **125** 1893 (1962).

[18] M. Mekata, J. Haruna, and H. Takaki, Localized magnetic moments in Mn_4N, J. Phys. Soc. Jpn. **21**, 2267 (1966).

[19] D. Fruchart, D. Givord, P. Convert, P. l'Heritier, and J. P. Sénateur, The non-collinear component in the magnetic structure of Mn_4N, J. Phys. F: Met. Phys. **9**, 2431 (1979).

[20] M. Uhl, S. F. Matar, and P. Mohn, *Ab initio* analysis of magnetic properties in noncollinearly ordered Mn_4N, Phys. Rev. B **55**, 2995 (1997).

[21] Y. Yasutomi, K. Ito, T. Sanai, K. Toko, and T. Suemasu, Perpendicular magnetic anisotropy of Mn_4N films on MgO(001) and $SrTiO_3$(001) substrates, J. Appl. Phys. **115**, 17A935 (2014).

[22] T. Hirose, T. Komori, T. Gushi, A. Anzai, K. Toko, and T. Suemasu, Strong correlation between uniaxial magnetic anisotropic constant and in-plane tensile strain in Mn_4N epitaxial films, AIP Adv. **10**, 025117 (2020).

[23] M. Meng, S. Li, M. Saghayezhain, E. W. Plummer, and R. Jing, Observation of large exchange bias and topological Hall effect in manganese nitride films, Appl. Phys. Lett. **112**, 132402 (2018).

[24] T. Bayaraa, C. Xu, and L. Bellaiche, Magnetization Compensation Temperature and Frustration-Induced Topological Defects in Ferrimagnetic Antiperovskite Mn_4N, Phys. Rev. Lett. **127**, 217204 (2021).

[25] P. Stamenov and J. M. D. Coey, Vector vibrating-sample magnetometer with permanent magnet flux source, J. Appl. Phys. **99**, 08D912 (2006).

[26] See Supplemental Material at http://link.aps.org/supplemental/10.1103/PhysRevB.106.L060409 for information about the XRR analysis, topological spin structure, and detailed analysis of the transport properties.

[27] D. Fruchart and E. F. Bertaut, Magnetic studies of the metallic perovskite-type compounds of manganese, J. Phys. Soc. Jpn. **44**, 781 (1978).

[28] V. T. N. Huyen, M.-T. Suzuki, K. Yamauchi, and T. Oguchi, Topology analysis for anomalous Hall effect in the noncollinear antiferromagnetic states of Mn_3AN (A = Ni, Cu, Zn, Ga, Ge, Pd, In, Sn, Ir, Pt), Phys. Rev. B **100**, 094426 (2019).

[29] H. Chen, Q. Niu, and A. H. MacDonald, Anomalous Hall Effect Arising from Noncollinear Antiferromagnetism, Phys. Rev. Lett. **112**, 017205 (2014).

[30] E. F. Bertaut, Representation analysis of magnetic structures, Acta Crystallogr. A **24**, 217 (1968).

[31] Z. Guguchia, J. A. T. Verezhak, D. J. Gawryluk, S. S. Tsirkin, J.-X. Yin, I. Belopolski, H. Zhou, G. Simutis, S.-S. Zhang, T. A. Cochran, G. Chang, E. Pomjakushina, L. Keller, Z. Skrzeczkowska, Q. Wang, H. C. Lei, R. Khasanov, A. Amato, S. Jia, T. Neupert, H. Luetkens, and M. Z. Hasan, Tunable anomalous Hall conductivity through volume-wise magnetic competition in a topological kagome magnet, Nat. Commun. **11**, 1 (2020).

[32] T. Miyasato, N. Abe, T. Fujii, A. Asamitsu, S. Onoda, Y. Onose, N. Nagaosa, and Y. Tokura, Crossover Behavior of the Anomalous Hall Effect and Anomalous Nernst Effect In Itinerant Ferromagnets, Phys. Rev. Lett. **99**, 086602 (2007).

[33] Z. Q. Liu, H. Chen, J. M. Wang, J. H. Liu, K. Wang, Z. X. Feng, H. Yan, X. R. Wang, C. B. Jiang, J. M. D. Coey, and A. H. MacDonald, Electrical switching of the topological anomalous Hall effect in a non-collinear antiferromagnet above room temperature, Nat. Electron. **1**, 172 (2018).

[34] H. Iwaki, M. Kimata, T. Ikebuchi, Y. Kobayashi, K. Oda, Y. Shiota, T. Ono, and T. Moriyama, Large anomalous Hall effect in $L1_2$-ordered antiferromagnetic Mn_3Ir thin films, Appl. Phys. Lett. **116**, 022408 (2020).